Spectral-domain magnetomotive OCT imaging of magnetic nanoparticle biodistribution

Amy L. Oldenburg[a,b], Vasilica Crecea[a,c], Stephanie A Rinne[a], Robabeh Rezaeipoor[a,b], Eric J. Chaney[a], Stephen A. Boppart[*a,b,c,d,e,f]
[a]Beckman Institute for Advanced Science and Technology, [b]Department of Electrical and Computer Engineering, [c]Department of Physics, [d]Department of Bioengineering, [e]Department of Medicine, University of Illinois at Urbana-Champaign, 405 N. Mathews Ave., Urbana, IL, USA 61801;
[f]Mills Breast Cancer Institute, Carle Foundation Hospital, 611 W. Park St., Urbana, IL, USA 61801;

ABSTRACT

Magnetomotive optical coherence tomography (MMOCT) is a method for imaging the distribution of magnetic nanoparticles in tissue by applying an external dynamic magnetic field gradient during B-mode scanning. We present a new method for spectral-domain MMOCT imaging which affords increased sensitivity and frame rates compared to previous work, with a demonstrated sensitivity to <100 ppm iron oxide nanoparticles and imaging time of 5 s. Agarose phantoms embedded with iron oxide nanoparticles (~20 nm) also provide negative T_2 contrast in magnetic resonance imaging (MRI) with sensitivity <10 ppm, which is promising for multi-modality applications where MRI and MMOCT provide whole-body and microscopic imaging, respectively. To demonstrate the biomedical potential of this technique, rats are injected with the same nanoparticles as those used in MRI, and uptake into the spleen is detected and imaged *post mortem* by MMOCT. This illustrates a potentially powerful multi-modal platform for molecular imaging using targeted magnetic nanoparticles.

Keywords: optical coherence tomography, contrast agents, magnetic nanoparticles, magnetomotive, magnetic resonance imaging, multimodal imaging

*boppart@uiuc.edu; phone 1 217 244-7479; http://biophotonics.uiuc.edu/

1. INTRODUCTION

Molecular imaging, that is, the ability to provide contrast to specific biomolecules, would greatly enhance the clinical utility of optical coherence tomography (OCT).[1,2] One approach is to develop intravenously administered nanoparticle contrast agents, which are surface labeled with antibodies or other proteins to target specific cell surface receptors. The first necessary step in this approach is to engineer nanoparticles and associated OCT imaging techniques which provide a large degree of contrast against the natural tissue background. The use of magnetic nanoparticles for this purpose has several advantages: the ability to externally manipulate the nanoparticles, the low magnetic susceptibility inherent in human tissues, the availability of FDA approved biocompatible iron oxide nanoparticles for MRI contrast, and the potential for hyperthermic therapy with high frequency (>100kHz) modulation.

In previous work we demonstrated the ability to image magnetite (Fe_3O_4) micro- and nanoparticles after uptake by *in vitro* macrophages[3] and *in vivo* African frog tadpoles[4] by modulating an externally applied magnetic field and detecting the resultant magnetomotion specific to the nanoparticles. Other researchers have also used this principle to provide hemoglobin contrast in optical Doppler tomography,[5] and to detect iron uptake in tissues with differential phase OCT[6] and also in ultrasound.[7] Recent results also suggest that the magnetomotive technique provides visco-elastographic information about the sample by resolving the spectral-domain OCT phase signal.[8]

Coherence Domain Optical Methods and Optical Coherence Tomography in Biomedicine XII,
edited by Joseph A. Izatt, James G. Fujimoto, Valery V. Tuchin, Proc. of SPIE Vol. 6847, 684719, (2008)
1605-7422/08/$18 · doi: 10.1117/12.761931

2. THEORY OF SPECTRAL DOMAIN MMOCT IMAGING

Because time-domain OCT (TDOCT) requires a mechanical optical delay arm, it is difficult to maintain a sufficient degree of phase correlation between successive axial scans in order to use phase-based detection of the nanoparticle motion. As a result, previous MMOCT methods have used amplitude-based detection (looking at changes in the envelope of the interferogram.) While this method was reasonably sensitive to a low concentration of nanoparticles [4], the use of a phase-sensitive method would be $f/\Delta f$ times more sensitive in the shot-noise limit, where $\Delta f / f$ is the fractional bandwidth of the light source. Also, because displacement is linearly related to the optical phase shift, the measurement of phase more easily provides quantitative displacement values (as opposed to cross-correlation methods required in amplitude detection). As shown in this work, spectral-domain OCT based on a line camera detection affords excellent phase stability and consequently pushes the sensitivity limits for MMOCT to even lower concentrations.

Previous work demonstrated a background-rejecting time-domain MMOCT (TDMMOCT) method by pulsing the magnetic field sequentially off-off-on at each transverse position. This allowed for a background displacement signal to be estimated from the difference between the off-off values. Then, by computing the difference between the off-on values and normalizing by the off-off difference, one could identify the magnetic-specific displacement, even in the presence of large motion artifacts such as respiration.[4] This was performed at a line rate of 10 Hz, providing the tissue sufficient time to mechanically equilibrate between each axial line acquisition. We find that in SDMMOCT using faster axial line rates (≥ 1 kHz), magnetomotion is dynamic,[8] and thus a new method which does not require excessive dwelling at each tissue location is needed. Instead, the electromagnet current $I(t)$ is continually modulated by a DC-offset sinusoid at frequency f_B:

$$I(t) = I_{\max}\sqrt{\frac{\sin(2\pi f_B t)+1}{2}} \tag{1}$$

(The DC offset is chosen to avoid the need for a polarity-switching power supply.) A square-root is used to achieve a resulting magnetic gradient force (proportional to the square of the magnetic field) that is a pure sinusoid with frequency f_B. This relationship is true as long as the magnetic field is sufficiently low such that the nanoparticles are below their saturation magnetization (magnetization is linear with respect to magnetic field). To couple the sinusoidal mechanical excitation with B-mode OCT scanning, we chose to modulate the magnetic field several cycles during the time taken to mechanically sweep the imaging light across one resolution length, which requires that:

$$f_B > \frac{v_{scan}}{\Delta x} \tag{2}$$

where v_{scan} is the transverse scan velocity, and Δx is the transverse image resolution. In this way, the transverse Fourier transform of the spectral-domain interferogram yields a magnetomotive signal at a higher frequency than the structural OCT image data band. In some sense this can be thought of as encoding a spatial channel (x) and a temporal channel (t) within different frequency bands of the same "image". Because the temporal channel is mixed by the low-frequency spatial channel (that is, the higher frequency magnetomotive signal is multiplied by the structural scattering signal), the bandwidth of the temporal channel is dictated by that of the spatial channel. To produce an MMOCT image, the raw image data is therefore bandpass-filtered about f_B with a bandwidth of $v_{scan}/\Delta x$, and subsequently inverse Fourier transformed. The normal OCT structural image can be obtained by transverse averaging or alternately low-pass filtering with a cutoff at $v_{scan}/\Delta x$. In this way, simultaneous structural and magnetomotive images can be obtained from one image. Because there will always be some noise at the magnetomotive frequency, it is also recommended to acquire a background image without magnetic field modulation.

3. EXPERIMENTAL METHODS

3.1 OCT imaging

Tissue phantoms designed to mimic both optical and mechanical soft tissues were prepared based on a mixture of cross-linking and non cross-linking silicone polymers as described previously.[4] We note a typo in reference [4]; phantoms were impregnated with 4 mg/g TiO_2 microparticles (not 4 μg/g) which provided a ~30 /cm scattering coefficient. Before oven curing at 80 °C, silicone solutions were mixed and sonicated with varying concentrations of magnetite (~25 nm, Sigma Aldrich) nanoparticles. The OCT imaging system consisted of a femtosecond laser (KMLabs) whose light output was coupled into a single-mode fiber interferometer, providing a 120nm bandwidth centered at 800 nm, and providing ~8 mW at the sample. A 40mm imaging lens provided 16μm transverse resolution, with axial resolution ~3 μm given by the coherence length of the light source. The water-cooled electromagnet provided ~600 G at the sample as described previously.[4] For TDMMOCT, a delay galvanometer was modulated at 10 Hz and dual-balanced detector (New Focus Nirvana) measured the interferogram. For SDMMOCT, a line scan camera (Dalsa Piranha) measured the spectral interferogram with an exposure time of 250 μs and linerate of 1 kHz. The image dimensions were kept at 0.5 mm wide by 0.75 mm deep for comparison, and the imaging times were 50 s for TDMMOCT and 5s (2.5 s each for control and modulated images) for SDMMOCT.

For tissue imaging, the same SDMMOCT parameters were used except a larger depth (1 mm) was analyzed. The MMOCT 2D image was computed by first computing the complex time-domain image (by taking the Fourier transform of the camera data along the spectral/axial dimension), then by applying a bandpass filter in the transverse/time dimension at $f_B \pm v_{scan}/\Delta x$. The filtered data for the magnetically modulated image was then divided by that from the control image, and the result was logarithmically scaled and median filtered before display.

3.2 MR imaging

Agar phantoms were prepared by mixing dH_20 with 40 mg/g agarose (Invitrogen), heating over 80 °C, combining with 0, 1, 3, 10 30, and 100 ppm concentrations of magnetite nanoparticles (Ocean Nanotech, 20 nm, COOH-terminated), loading the mixtures into 5 mm diameter NMR tubes cut to 1 inch lengths, and allowing them to gel at room temperature. Phantoms were subsequently imaged in cross-section using spin-echo MRI at the Beckman Biomedical Imaging Center, Urbana, IL, with a 4.7 T 200 MHz Varian SISCO. The repetition rate was fixed at T_R = 4 s, slice thickness 10 mm, and two images were taken with echo times of T_E = 11 ms and 50 ms. A $CuSO_4$ marker was used to mark the orientation of the phantoms in the image.

3.3 PEGylation of magnetic nanoparticles for intravenous administration

Purified, 20 nm iron oxide nanoparticles terminated with carboxyl groups were obtained from Ocean NanoTech, LLC. A solution was prepared with 0.13 mg/mL nanoparticles in 10 mM 2-(N-morpholino)ethanesulfonic acid buffer (pH 6, Aldrich), 30 μM 1-(3-Dimethylaminopropyl)-3-ethylcarbodimide hydrochloride (Pierce Biotechnology) and 30 μM *N*-hydroxysulfosuccinimide sodium salt (Pierce Biotechnology). The solution was kept at room temperature for 20 minutes to activate the carboxyl groups of the nanoparticles. The pH was then brought to 7.4 with 0.1 M NaOH (Aldrich) and polyethylene glycol monoamine (2.5 μM, 2,000 Mw, supplied by Ocean Nanotech, LLC) was quickly added. The solution was incubated at room temperature for 2 hours and purified via ultracentrifugation (Beckman Optima TL 100) or centrifugal filtration (100,000 MWCO, Millipore Ultrafree-CL). All chemicals were used as received.

3.4 Animal model

PEGylated nanoparticles were distributed in saline (0.9% NaCl) at a nominal concentration of 1 mg/mL, and injected into the tail vein of a Wistar-Furth inbred rat (Jackson Labs, Bar harbor, ME). The total nanoparticle dosage is estimated to be ~0.5 mg/kg Fe. After 2 hours circulation time, the rat was euthanized by CO_2 inhalation, and the major organs were harvested and frozen at -80 °C. A control rat was treated identically except by injection with a similar volume of saline only. All procedures were carried out according to protocols approved by the Institutional Review Board of the University of Illinois at Urbana-Champaign.

4. RESULTS AND DISCUSSION

4.1 SDMMOCT of tissue phantoms

Images were acquired of opto-mechanical tissue phantoms with various magnetic particle concentrations. We can immediately observe the effects of the sinusoidal magnetomotion on the raw spectral interferograms as a function of time, which are displayed in Fig. 1. We can clearly see that some lower-frequency modulations are present in the field off image which are due to scattering structures in the object being transversely scanned. In the magnetically modulated image, however, a higher frequency due to the magnetomotion is now mixed with the scattering structural signal.

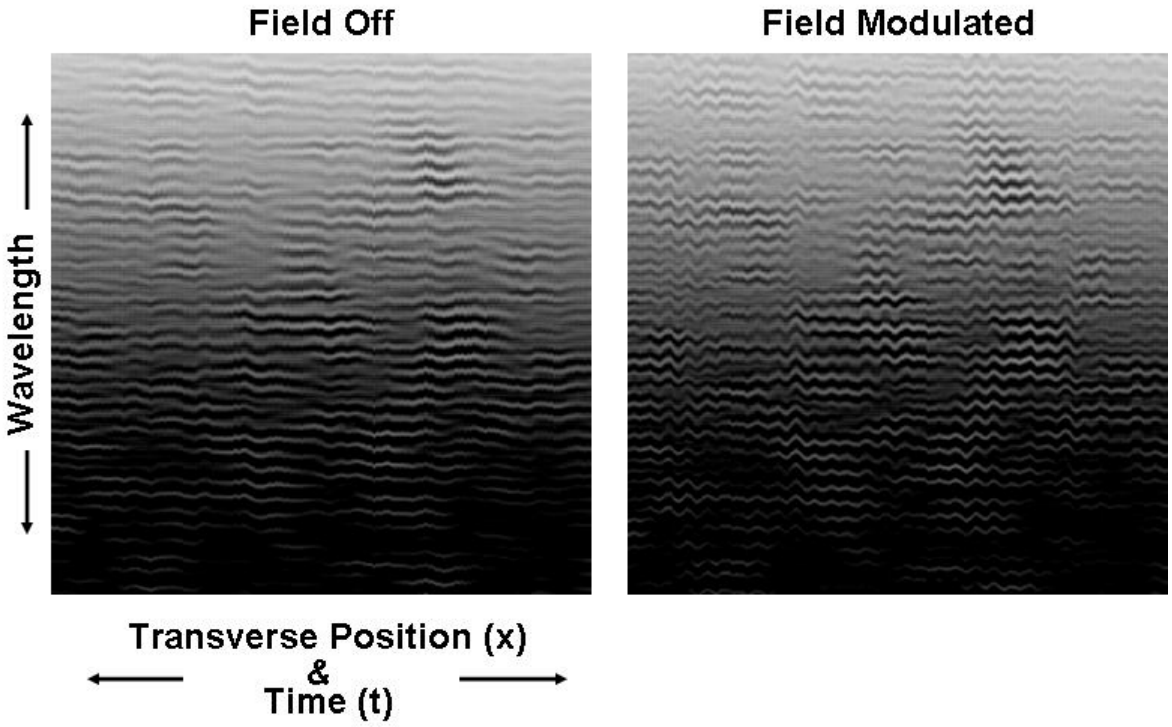

Fig. 1. A zoomed-in portion of the raw spectral interferograms (vertical dimension) acquired as a function of transverse position and time (horizontal dimension), for an image with the magnetic field off (left) and modulated (right).

Example transverse Fourier spectra of the raw spectral-domain image data are shown in Fig. 2. For each sample, a pair of images were acquired with and without magnetic field modulation at f_B = 100 Hz, which is well above $v_{scan}/\Delta x$ = 12.5 Hz. We find in practice that during transverse scanning across our imaging lens, a phase ramp is applied which downshifts the modulation signals by 30 Hz. However, this effect is predictable, and M-mode images exhibit no downshifting. As shown in Fig. 2, a large magnetomotive component at 70 Hz is observed which is more than a decade above the signal from a background image (with no magnetic field modulation). The large low frequency component (<50 Hz) contains all of the usual OCT structural image information.

We also find that for higher magnetic particle concentrations, harmonics of f_B appear, as shown in the lower panel of Fig. 2. This can be explained by the fact that the phase predominantly carries the magnetomotive modulation term in the OCT interferogram:

$$\begin{aligned} A_{OCT}(t) &= A_0 \exp\left(i\phi_0 + i\left(4\pi n\Delta z / \lambda\right)\sin\left(2\pi f_B t\right)\right) \\ &\approx A_0 \exp\left(i\phi_0\right)\left\{1 + i\left(4\pi n\Delta z / \lambda\right)\sin\left(2\pi f_B t\right)\right\} \quad for \quad n\Delta z << \lambda \end{aligned} \tag{3}$$

where A is the complex analytic signal produced by Hilbert transformation of the raw image data, λ is the center wavelength of the light source, and n is the refractive index of the medium. We note that A is therefore a Bessel

function of the first kind exhibiting harmonics of f_B for sufficiently large displacements Δz. For displacements small with respect to the wavelength, the response is approximated as a simple sinusoid using the small-angle approximation. We note that it is possible to compute the phase angle of the complex image data A and perform Fourier analysis directly on this parameter, which would get rid of the undesired Bessel mode artifacts. However, one nice feature of spectral analysis of the direct signal A is that the magnetic modulation signal is automatically scaled by the overall signal amplitude (scattering signal) of the sample. Thus, it is a simple way to preferentially weight signals that are well above the noise floor of the image.

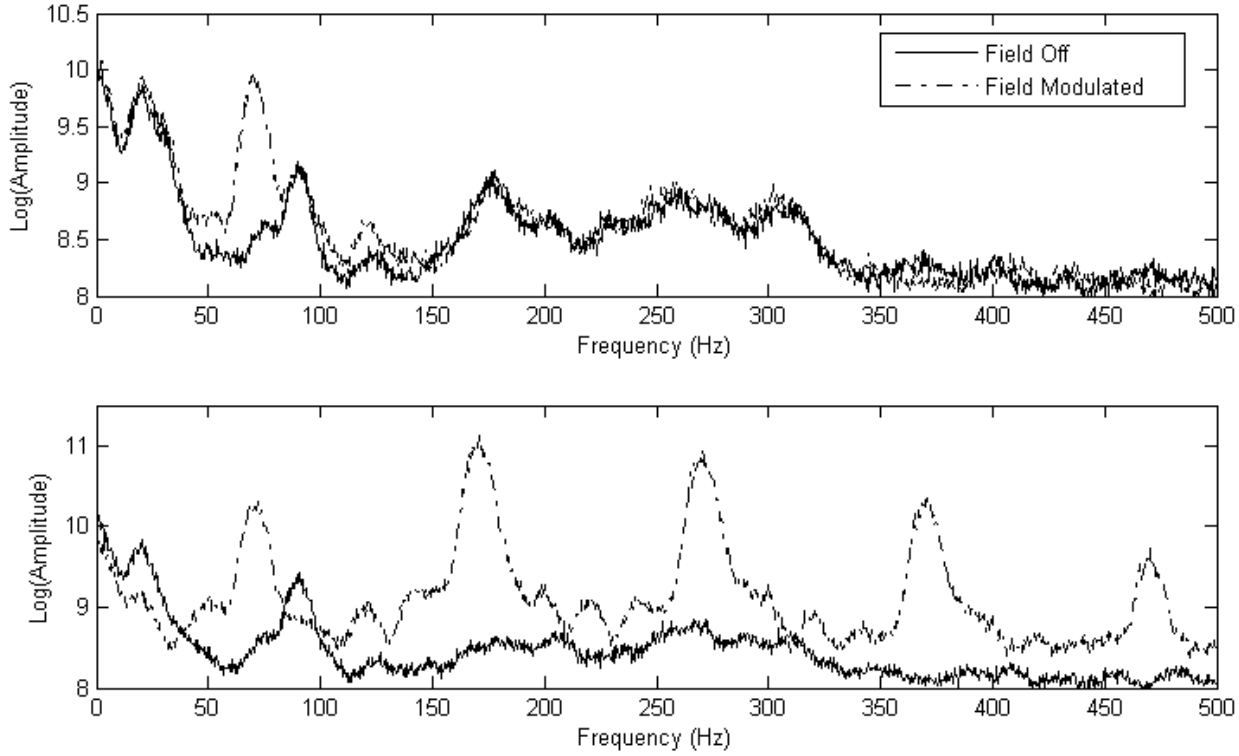

Fig. 2. Image-averaged transverse Fourier transforms for tissue phantoms with 120 ppm nanoparticles (top) and 930 ppm nanoparticles (bottom), with f_B = 100 Hz and a downshift of -30 Hz due to the lens.

We can define the signal-to-noise ratio (SNR) of the magnetomotive signal as the integrated transverse spectral intensity across $f_B \pm v_{scan}/\Delta x$ divided by that from the control without the applied field. We find that the SNR is greatly improved from the previous TDMMOCT system using the 3-pulse method.[4] The concentration-dependent SNRs are shown in Figure 3. While TDMMOCT affords a sensitivity to only 500 ppm magnetite nanoparticles, the SDMMOCT system detected phantoms with ~50 ppm nanoparticles. This is because the SDMMOCT interferogram is phase-sensitive, whereas the TDMMOCT data is demodulated to remove the phase contribution (because the moving delay arm decorrelates the phase between successive axial scans). The non-zero control value for the SDMMOCT data is likely due to diamagnetic repulsion of the background matrix. Saturation of the SDMMOCT SNR at higher nanoparticle concentrations occurs when the modulation signal shifts into the harmonics of f_B and the displacements are no longer small with respect to the wavelength.

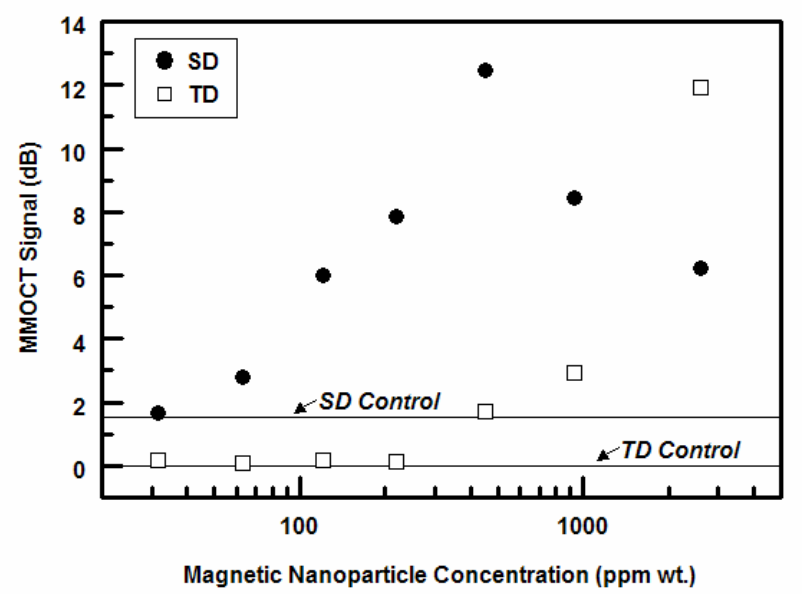

Fig. 3. Comparison of concentration-dependent SNR for SD (spectral domain) and TD (time domain) MMOCT. Horizontal lines indicate the SNRs of the control phantom for each technique.

4.2 MR imaging of tissue phantoms

The results of MR imaging of phantoms containing varying concentrations of magnetite nanoparticles are shown in Table 1. These can be understood by writing the SNR for spin-echo imaging as a function of the spin-lattice relaxation time T_1 and the spin-spin relaxation time T_2 of the system:

$$SNR \propto \left(1-\exp\left(-\frac{T_R}{T_1}\right)\right)\exp\left(-\frac{T_E}{T_2}\right) \tag{4}$$

where T_E is the echo time and T_R the repetition time used during imaging. We see that the SNR is decreased as the concentration of the nanoparticles is increased (a negative contrast effect). When the echo time was increased to 50 ms from 11 ms, we observe a more dramatic decrease in SNR with increasing nanoparticle concentration. Because of this strong echo time dependence on the concentration-dependent SNR, we see from Eq. (4) that the nanoparticles must be shortening T_2. Thus, as we might expect, these nanoparticles are negative T_2 contrast agents. The sensitivity levels appear to be on the order of 10 ppm when using longer echo times.

Table 1. The SNR of spin-echo MRI of agar phantoms for two different echo times T_E are displayed as a function of the magnetic nanoparticle concentration.

Magnetic Nanoparticle Concentration	Signal-to-noise ratio	
	T_E = 11 ms	T_E = 50 ms
0 ppm	26.1	14.2
1 ppm	25.5	13.3
3 ppm	24.9	10.1
10 ppm	19.6	3.5
30 ppm	9.4	1

4.3 Nanoparticle uptake in an animal model

The spleen was chosen as a likely organ in the reticuloendothelial system to which nanoparticles of 20 nm size would accumulate. The spleens of both the saline control and nanoparticle-injected rats were imaged using B-mode SDMMOCT in six locations while stepping across the long axis of the organ. Both control and modulated images were acquired at each location, with f_B = 100 Hz. The magnetic-specific SNR was computed for both groups using the same technique as for the phantoms above. The control spleen images exhibited an SNR of 0.095 ± 0.29 dB. The nanoparticle-laden spleen images exhibited an SNR of 0.62 ± 0.42 dB, which is separated from the control group by about 1 standard deviation. Four of the 6 nanoparticle-laden spleen images exhibited an SNR greater than 1 standard deviation above the control. Figure 4 displays representative images from the two groups, where the structural OCT image is displayed alongside its associated MMOCT image, computed according to the methods outlined above. Specific hot spots were observed in certain regions of the nanoparticle-laden spleen only.

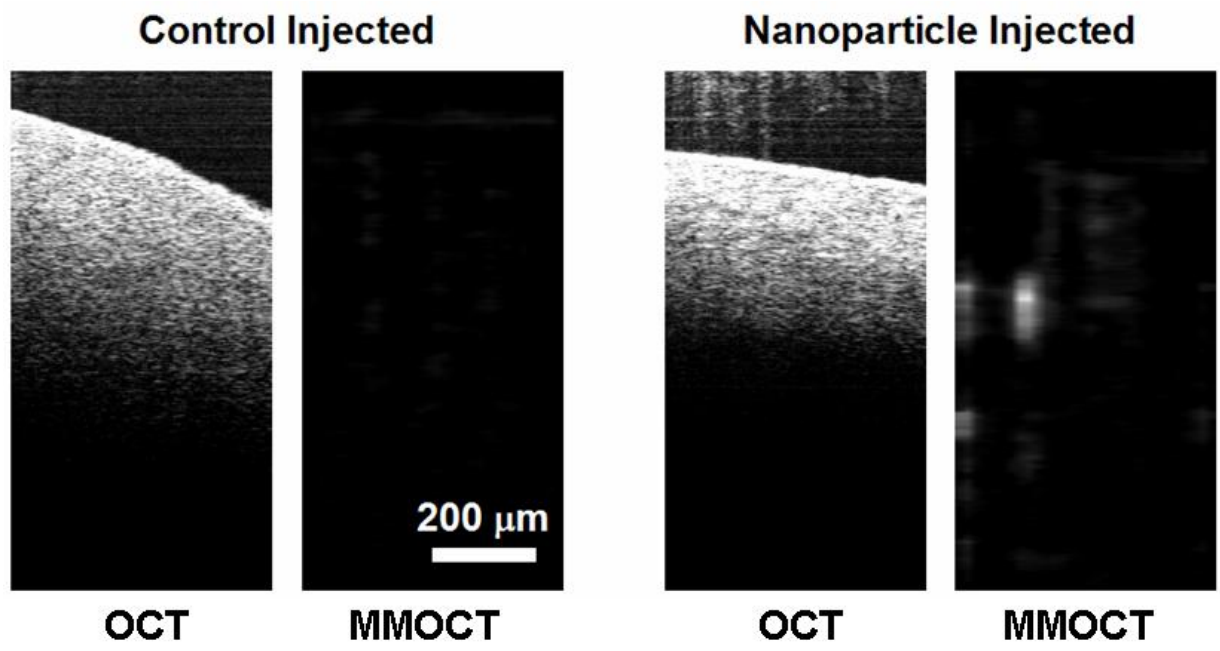

Fig. 4. Representative structural (left panels) and corresponding magnetomotive (right panels) OCT images of *post mortem* rat spleens. MMOCT images are constructed by bandpass filtering the data in the transverse dimension at the frequency of the magnetic field modulation.

5. SUMMARY AND CONCLUSIONS

We describe a new method for imaging the distribution of magnetic nanoparticles with extremely high sensitivity (< 100 ppm) that is capable of detecting natural nanoparticle uptake in the reticuloendothelial system of a wild type rat post tail-vein injection, using a dosage less than that used in humans for MRI contrast (2.8 mg/kg Fe). We also demonstrate the same nanoparticles which provide SDMMOCT contrast are also excellent MRI contrast agents (< 10 ppm sensitivity). This is promising for future molecular imaging studies which may take advantage of simultaneous whole-body and microscale imaging afforded by MRI and MMOCT, respectively.

ACKNOWLEDGEMENTS

We would like to thank Dr. Daniel Marks at the University of Illinois for his assistance with OCT, and Boris Odintsov at the Biomedical Imaging Center at the University of Illinois for assistance with MRI. This work was

supported in part by the National Institutes of Health (NIBIB 1 R01 EB001777, and Roadmap 1 R21 EB005321, NIBIB, 1 R01 EB005221, and NIBIB 1 R01 EB001777).

REFERENCES

[1] C. Yang, "Molecular contrast optical coherence tomography: A review", Photochem. Photobiol. **81**, 215 (2005).
[2] S. A. Boppart, A. L. Oldenburg, C. Xu, D. L. Marks, "Optical probes and techniques for molecular contrast enhancement in coherence imaging," J. Biomed. Opt. **10**, 041208 (2005).
[3] A. L. Oldenburg, J. R. Gunther, S. A. Boppart, "Imaging magnetically labeled cells with magnetomotive optical coherence tomography," Opt. Lett. **30**, 747 (2005).
[4] A. L. Oldenburg, F. J.-J. Toublan, K. S. Suslick, A. Wei, S. A. Boppart, "Magnetomotive contrast for *in vivo* optical coherence tomography," Opt. Express **13**, 6597 (2005).
[5] J. Kim, J. Oh, T. E. Milner, J. S. Nelson, "Hemoglobin contrast in magnetomotive optical Doppler tomography," Opt. Lett. **31**, 778 (2006).
[6] J. Oh, M. D. Feldman, J. Kim, H. W. Kang, P. Sanghi, T. E. Milner, "Magneto-motive detection of tissue-based macrophages by differential phase optical coherence tomography," Lasers Surg. Med. **39**, 266 (2007).
[7] J. Oh, M. D. Feldman, J. Kim, C. Condit, S. Emalianov, T. E. Milner, "Detection of magnetic nanoparticles in tissue using magneto-motive ultrasound," Nanotech. **17**, 4183 (2006).
[8] V. Crecea, A. L. Oldenburg, T. S. Ralston, S. A. Boppart, "Phase-resolved spectral-domain magnetomotive optical coherence tomography," Proc. SPIE 6429, 64291X (2007).